

# Chapter 3

## Data analysis

### 3.1 Neutron energy calculation

High energy neutrons were generated when natural lithium foil was bombarded with the proton of 10, 13, 15, 16, 18, 19, 21 and 22 MeV energies, these quasi-mono energetic neutrons were produced in the forward direction via the  $^{nat}\text{Li}(p,n)$  reaction in the present experimental setup. The present experiment was conducted for natural Lithium target so the contribution for  $^6\text{Li}$  was obtained using spectral shape, cross section and neutron yields given in Ref. [1]. The contributions of  $^{6,7}\text{Li}$  were added as per natural abundance and final spectra were obtained. The threshold for  $^7\text{Li}(p,n)$  is 1.8 MeV and it is 5.9 MeV for  $^6\text{Li}(p,n)$ , therefore  $^6\text{Li}$  contributes ~2% at  $E_p = 18$  and 19 MeV and ~5% at  $E_p = 21$  and 22 MeV around 4 MeV below the major peak from  $^7\text{Li}$  nuclei. The contribution from  $^6\text{Li}$  is negligible at 10, 13, 15 and 16 MeV proton energies. This reaction  $^7\text{Li}(p,n)$  produces monoenergetic neutrons below the proton energy of 2.4 MeV. However, above the proton energy of 2.4 MeV, the first excited state of  $^7\text{Be}$  is populated 0.43 MeV above the ground state, which generated the second group of neutrons along with the primary neutrons. The  $^7\text{Be}$  ground state threshold is 1.88, and neutron energy corresponding to the ground state is  $E_p - 1.88$ . Similarly, the first excited state threshold for  $^7\text{Be}$  is 2.38 MeV, and neutron energy corresponding to the first excited state is  $E_p - 2.38$ . In the  $^7\text{Li}(p,n)$  reaction, for the proton energy below 5 MeV at zero-degree, these low energy neutrons yield less than about 10% of the ground state yield. Thus, the usefulness of the mono energetic neutron source is only slightly impaired. The three-body breakup reaction  $^7\text{Li}(p,n + 3\text{He})^4\text{He}$  occurs above 3.68 MeV, which populates excited states of  $^7\text{Be}$  and contributes to neutron with primary neutron peak. The two peaks visible below the major peak correspond to the  $5/2^-$  and  $7/2^-$  resonant breakup reaction and further lower part of the spectra is generated from contribution to the continuum [2]. These different neutron production reaction channels along with the threshold for proton induced reaction on natural lithium are mentioned in Table 3.1. The primary neutron peak has higher neutron energy and flux, and this peak is used to measure the  $(n, 2n)$

and  $(n, p)$  reactions cross section of Se, Sb, V, Cu and Rh isotopes. The neutron flux spectra for 10, 13, 15, 16, 18, 19, 21 and 22 MeV proton energies were obtained by interpolation techniques using the neutron flux spectra of the C. H. Poppe *et al.* [3] at 10 MeV and M. W. McNaughton *et al.* [4] at 15 and 20 MeV proton energies as shown in Fig. 3.1. The neutron distribution has a quasi-monoenergetic peak near  $E_p - 1.88$  and long tailing towards lower energies is shown in Fig. 3.1. This neutron spectrum was used for the neutron energy calculation based on the kinematic relation ( $E_n = E_p - E_{th}$ ), where  $E_p$  is the proton energy, and  $E_{th}$  is the threshold energy of the  ${}^7\text{Li}(p, n)$  reaction. The effective mean neutron energy of the primary neutron group from the neutron spectrum was calculated using equation (1) as mentioned in the D. L. Smith *et al.* [5] and uncertainty associated with this neutron energy is the spectrum width of the primary neutron peak. The calculated neutron energy is given as  $7.87 \pm 0.58$ ,  $10.50 \pm 0.68$ ,  $12.50 \pm 0.68$ ,  $13.52 \pm 0.67$ ,  $15.79 \pm 0.55$ ,  $16.86 \pm 0.55$ ,  $18.87 \pm 0.59$  MeV and  $19.81 \pm 0.59$  corresponding to 10, 13, 15, 16, 18, 19, 21 and 22 MeV proton energies.

$$\langle E_n \rangle = \frac{\int_{E_{ps}}^{E_{max}} E_i \phi_i(E) dE}{\int_{E_{ps}}^{E_{max}} \phi_i(E) dE} \quad (1)$$

$\langle E_n \rangle$  is the effective mean neutron energy,  $E_{max}$  is the maximum neutron energy,  $E_{ps}$  is the peak forming start energy,  $E_i$  is the energy bin and  $\phi_i(E)$  is the neutron flux for the energy bin  $E_i$ .

**Table 3.1** The different neutron production reaction channels for the  ${}^{\text{nat}}\text{Li}(p, n)$  reaction.

Sr. No	Reaction	Q-Value (MeV)	$E_{th}$ (MeV)
1	${}^6\text{Li}(p, n){}^6\text{Be}$	-5.07	5.92
2	${}^6\text{Li}(p, np){}^5\text{Be}$	-5.67	6.62
3	${}^7\text{Li}(p, n){}^7\text{Be}$ (Ground state transition)	-1.644	1.88
4	${}^7\text{Li}(p, n){}^7\text{Be}^*$ (First excited-state transition)	-2.079	2.38
5	${}^7\text{Li}(p, n){}^3\text{He}{}^4\text{He}$ (Three-body break up reaction)	-3.23	3.68
6	${}^7\text{Li}(p, n){}^7\text{Be}^{**}$	-6.18	7.06

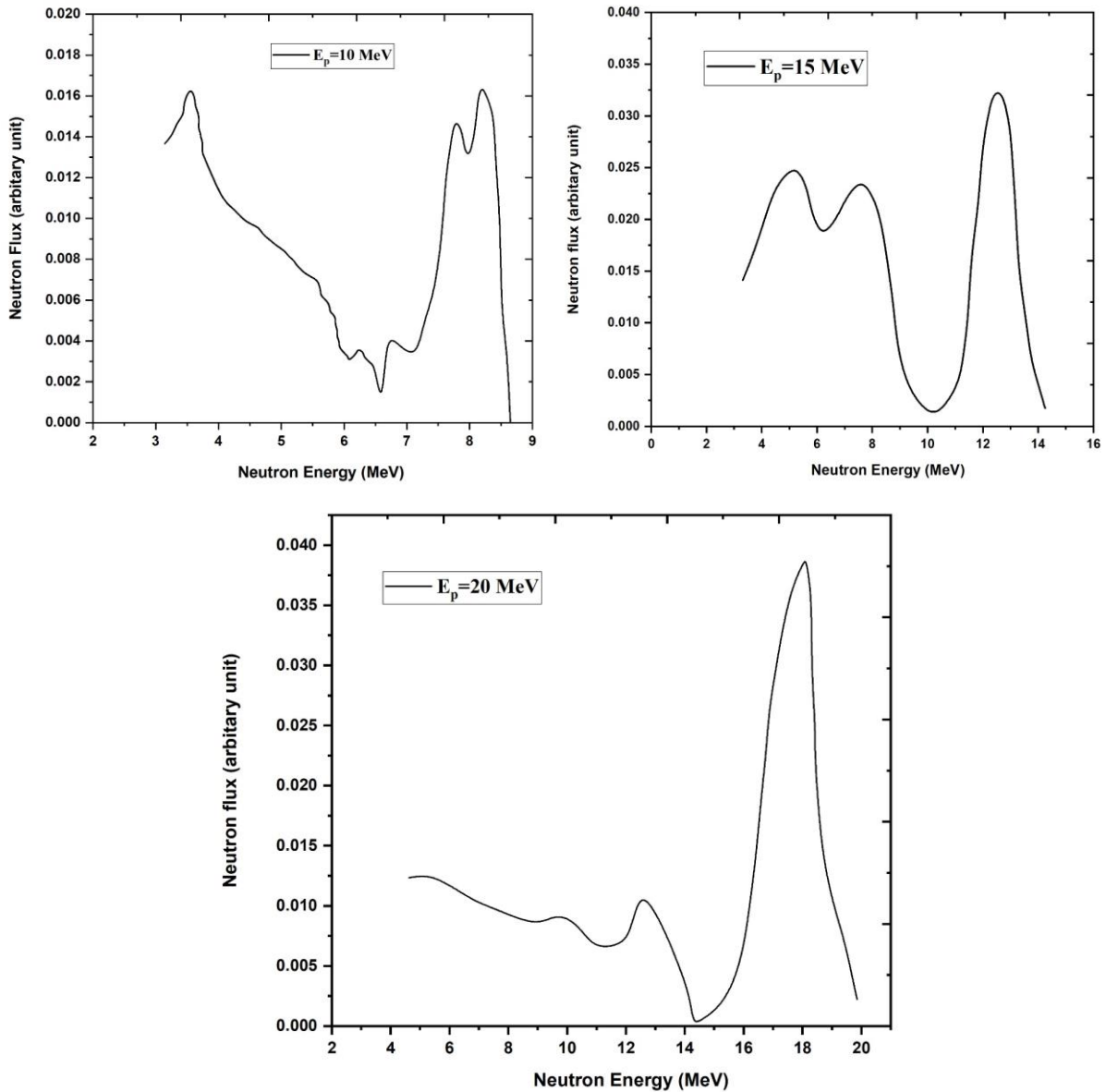


*Fig. 3.1 The neutron flux spectrum produced by the  $^{nat}\text{Li}(p, n)$  reaction at  $0^\circ$  of the 10, 15 and 20 MeV proton energies are obtained from the reference data of the C. H. Poppe et al. [3] and M. W. McNaughton et al. [4].*

## 3.2 Efficiency and energy calibration of the HPGe detector

### 3.2.1 Energy calibration of the HPGe detector

The adjustment of the **H**igh **P**urity **G**ermanium (HPGe) detector to a well-defined precise and optimum performance condition is necessary for the off-line  $\gamma$ -ray spectroscopy and this can be achieved by properly adjusting the associated electronic modules. An

important unit is a spectroscopic amplifier. The HPGe detector is used in situations where isotope identification is needed because of the excellent resolution. The detector resolution can be best achieved by properly adjusting the shaping time of the spectroscopy amplifier. The detector resolution is defined as the full width at half maximum (FWHM) divided by their peak centroid for a given photon in a spectroscopy amplifier.

$$Resolution = \frac{(FWHM)}{(Peak)} \times 100 (\%) \quad (2)$$

The FWHM of the spectrum peak depends on the shaping time. A short shaping time does not include all the preamplifier pulses and a long shaping time includes too much signal noise. The best FWHM is obtained with the shaping time suited to the detector preamplifier output signal. The variation of the FWHM is carefully studied with the variation in the shaping time of the spectroscopy amplifier. In this way, an optimum and best resolution was obtained with a suitable shaping time. The next task is to calibrate the Multi-Channel Analyzer (MCA) initially, this is done with the help of a standard  $\gamma$ -ray like  $^{152}\text{Eu}$  point source. The device is used to process the electronic pulses generated by an HPGe detector and energy spectra are stored in the device memory for further retrieval and analysis on a computer. The spectral memory of the MCA is up to 4096 channels. The prominent peaks in the background also serve as additional points. To check the calibration using a multi  $\gamma$ -ray source like  $^{152}\text{Eu}$  is preferred because it covers the  $\gamma$ -ray energies from 122 keV to 1408 keV. This energy region almost covers the region of interest in the present studies. Once the calibration is done, the energy of any unknown peak appearing in the  $\gamma$ -spectrum can be obtained with the help of the calibration equation [6]. Normally for the limited region 100 to 1500 keV, a linear relation is assumed between the photon energy and the centroid of the peak weighted least square fitting of the calibration points gives the equation:

$$E (keV) = a + b * channel + c * channel^2 \quad (3)$$

Where  $a$ ,  $b$  and  $c$  are the fitting parameters and the values of these parameters are as follows:  $-0.5616$ ,  $0.4494$  and  $-2.43 \times 10^{-7}$ . The energy calibration curve of the HPGe detector is shown in Fig. 3.2.

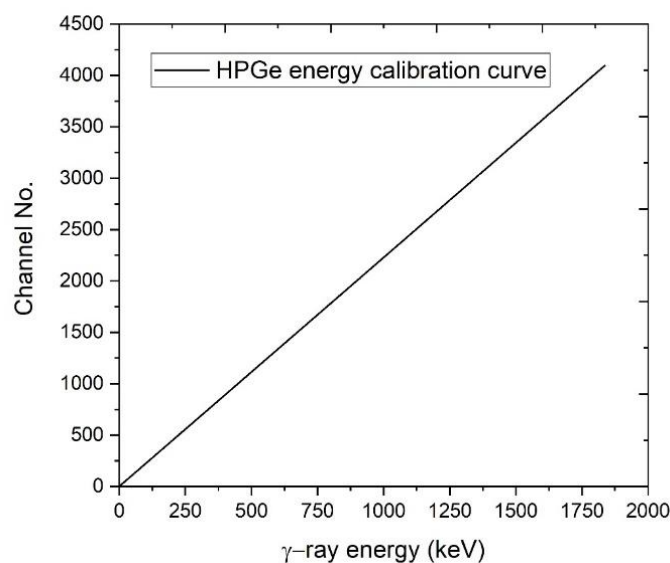


*Fig. 3.2 the energy calibration curve of the HPGe detector.*

### **3.2.2 Efficiency calibration of the HPGe detector**

The efficiency of the HPGe detector is an essential quantity for the determination of the reaction cross sections. The accuracy of the determination of the efficiency will influence the accuracy of the overall measurement. Hence, there are several points to be considered while determining the efficiency of an HPGe detector. The first thing is geometry, one must select a suitable geometry of the source and detector. The second thing is source, the use of a multi gamma source. It is advantageous to use a multi  $\gamma$ -ray source, which emits  $\gamma$ -rays with different energies spread over the entire range of interest. Several such sources have been proposed in the literature. Concerning half-life  $^{152}\text{Eu}$  source is particularly suited for the energy region 100 to 1500 keV. The details of this nuclide are given in Table 3.2.

As taken from literature  $\gamma$ -ray spectroscopy is widely used for the determination of the  $\gamma$ -ray emission rates. The high accuracy was obtained by considered of coincidence summing corrections. Coincidence summing occurs with radionuclides emitting two or more cascading photons within the resolving time of detector. If the first photon spends its total energy in the Ge crystal and the second photon is also detected, a sum peak which may not correspond to either of the two full energy peaks is recorded, the probability for such summing effects decreases with an increasing source to detector distance, i.e., by using small solid angles of the detector. So, by properly adjusting the count rates and geometry, the losses due to dead

time, pile up, and cascading effects can be reduced [7]. The efficiency of the HPGe detector is calculated by formula given as follows:

$$\epsilon = \frac{A K_c}{C L I_\gamma N_0 e^{-\lambda t}} \quad (4)$$

Where  $A$  is the area of the peak,  $I_\gamma$  is the gamma-ray intensity,  $K_c$  is the correction factor,  $N_0$  is the activity at the time of calibration,  $\lambda$  is the decay constant. The efficiencies were interpolated through the following fitting function:

$$\epsilon(E) = \epsilon_0 * \exp(-E/E_0) + \epsilon_c \quad (5)$$

Where  $\epsilon_0$ ,  $E_0$  and  $\epsilon_c$  are the fitting parameter and values along with calculate efficiencies for characteristics  $\gamma$ -lines of 468.6 for  $^{102}\text{Rh}^g$ , 697.5, 766.8, 1112.8, 1112.8 for  $^{102}\text{Rh}^m$ , 1115.53 for  $^{65}\text{Ni}$  and 1368.62 keV for  $^{24}\text{Na}$  are given in Table 3.3. The two different irradiations were performed and fitted efficiency curve of the HPGe detector with and without correction factor ( $K_c$ ) is shown in Fig. 3.3 as follow:

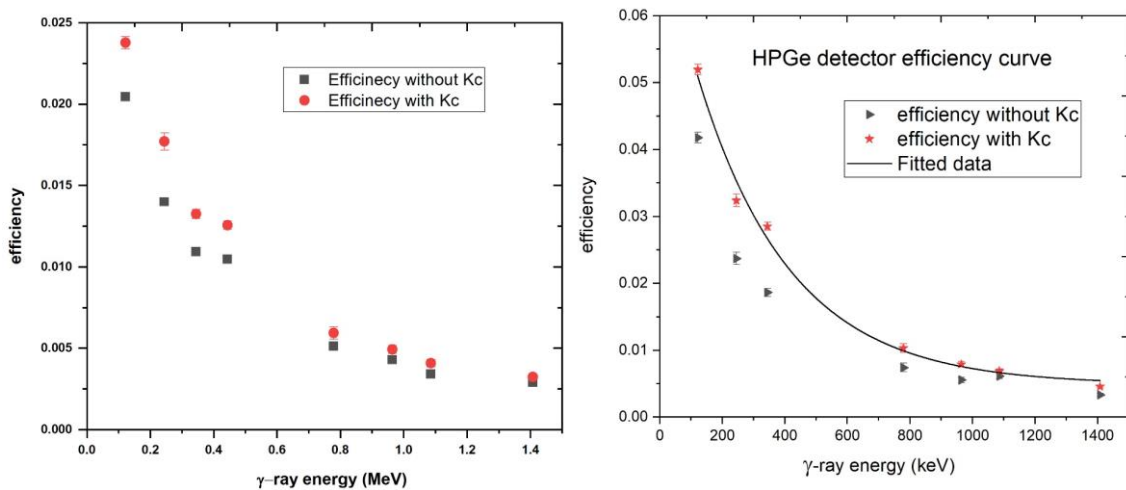


**Fig. 3.3** The efficiency calibration curve of the HPGe detector with and without coincidence summing effect correction factor  $K_c$  of the HPGe detector for the  $^{152}\text{Eu}$  source.

**Table 3.2** The  $\gamma$ -ray energies of the  $^{152}\text{Eu}$  sources [8].

$\gamma$ -ray from $^{152}\text{Eu}$ (13.537 y (6))		
$E_\gamma$ (keV)	$I_\gamma$ (%)	Decay mode
121.78	28.58 (6)	$e+b+$
344.278	26.5 (4)	$\beta^-$
1408.006	21.005 (24)	$e+b+$

964.079	14.605 (21)	$e+b+$
1112.074	13.644 (21)	$e+b+$
778.9040	12.942 (19)	$\beta^-$
1085.869	10.207 (21)	$e+b+$
244.6975	7.583 (19)	$e+b+$
867.378	4.245 (19)	$e+b+$
443.965	2.821 (19)	$e+b+$
411.1163	2.234 (4)	$\beta^-$
1089.737	1.727 (6)	$\beta^-$
1299.140	1.623 (8)	$\beta^-$
1212.948	1.422 (6)	$e+b+$

**Table 3.3** Measured values of fitting parameters of the HPGe detector efficiencies.

Fitting parameters	parameter values	$E_\gamma$ (keV)	Efficiencies
$\varepsilon_0$	$0.06751 \pm 0.00373$	468.6	0.01926
		697.5	0.01153
$\varepsilon_c$	$0.00377 \pm 0.0007243$	766.8	0.01014
$E_0$	$335.39 \pm 32.384$	1112.8	0.0065
		1115.53	0.0062
		1368.63	0.004914

### 3.3 Offline $\gamma$ -ray activity measurements

The samples were irradiated at 2.1 cm from the neutron source for 7 to 9 hours to obtain sufficient activity in the samples and the reference foils. After the irradiation process the samples were taken out after sufficient cooling and mounted on different Perspex plates for counting in front of a lead shielded high purity germanium (HPGe) detector. This detector was shielded with lead blocks to reduce the contribution of the natural background radioactivity. These samples were placed at 3 cm from the detector window in the low background counting facility of the TIFR-RCD lab for activity measurements. At this distance, the end cap of the detector the dead time was less than 2% which also minimize the coincidence summing effect. The relatively close geometry was used in the present work to enhance the counting rate. At very close geometry, the correction factor related to

coincidence summing effects was taken into consideration. The  $\gamma$ -ray activity from the sample was measured using a pre-calibrated HPGe detectors coupled to a PC-based 4096 multi-channel analyzer (MCA) and the CAMAC based Genie-2000  $\gamma$ -ray spectroscopy software was used for the data acquisition.

The p-type coaxial high-purity germanium detector HPGe detector manufactured by Baltic Scientific Instruments (BSI) was used in the present work for the activity measurements of the samples and reference foils, whose model is GCD-40190. The relative efficiency of this HPGe detector was 40% and energy resolution was 895 eV at 122 keV and 1.9 keV at 1.33 MeV. The experimental setup of this BSI HPGe detector is shown in Fig. 3.4 for activity measurements. Similarly, the measurements of induced activity were performed for the samples and reference foils after the end of each irradiation by a 16% relative efficiency pre-calibrated Canberra p-type coaxial high-purity germanium (HPGe) detector coupled to a PC-based 4096 multi-channel analyzer.



*Fig. 3.4 The HPGe detector which is properly shielded by lead reduces the contribution of natural radioactivity.*

The detector efficiency and energy calibration were carried out using a  $^{152}\text{Eu}$  radioactive point source that is standard and well-characterized and a typical  $\gamma$ -ray spectrum of a  $^{152}\text{Eu}$  point source obtained by an HPGe detector is presented in Fig. 3.5. Similarly, the  $\gamma$ -ray spectrum for activated samples and monitor at different neutron energies along with the irradiation, cooling and counting time are shown in Fig. 3.6.

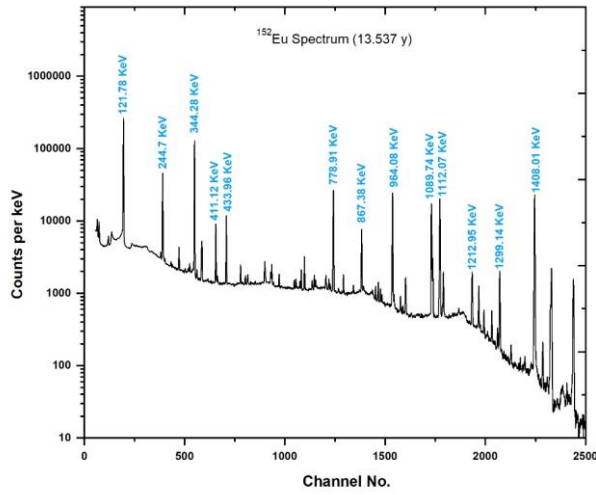
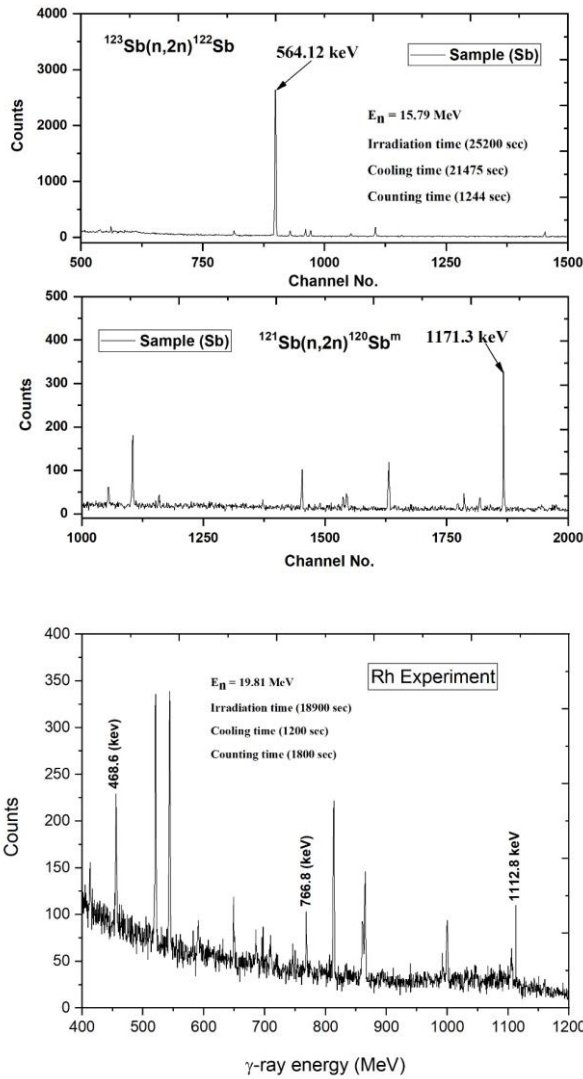
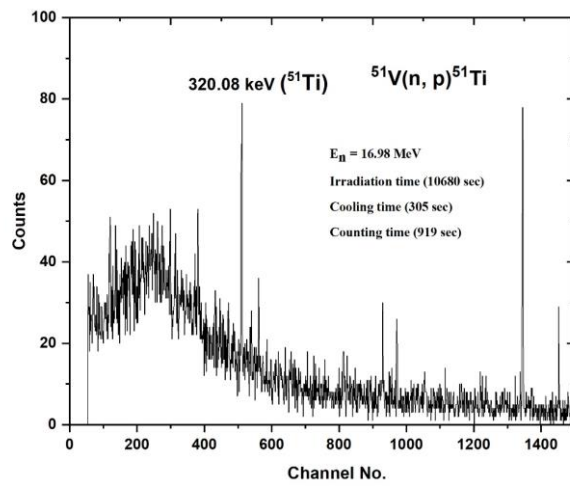
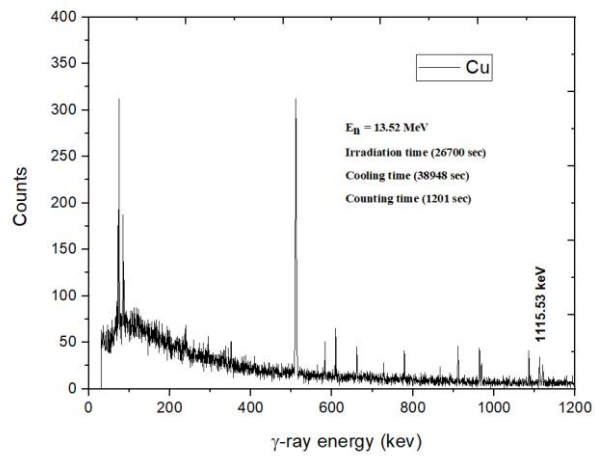
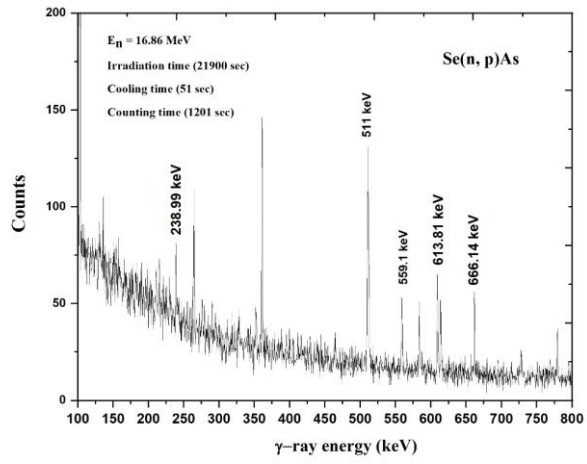
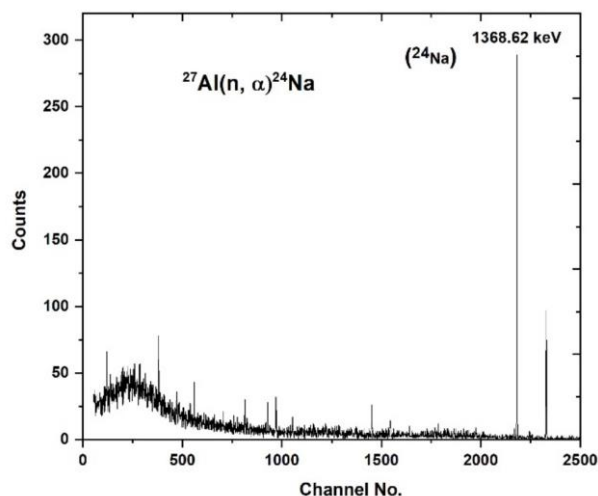


Fig. 3.5 The off-line  $\gamma$ -ray spectrum of a  $^{152}\text{Eu}$  point source obtained with an HPGe detector.







**Fig. 3.6** Off-line  $\gamma$ -ray energy observed after the neutron irradiation. The  $\gamma$ -ray transitions from the decay of the Ti, Ni, Rh, Sb, As and Na nuclei have been marked.

The spectroscopic decay data half-life of the reaction product, decay mode, energy and intensity of  $\gamma$ -lines and target isotopes abundance of the radioisotopes  $^{24}\text{Na}$ ,  $^{51}\text{Ti}$ ,  $^{65}\text{Ni}$ ,  $^{76}\text{As}$ ,  $^{77}\text{As}$ ,  $^{78}\text{As}$ ,  $^{80}\text{As}$ ,  $^{102}\text{Rh}^g$ ,  $^{102}\text{Rh}^m$ ,  $^{120}\text{Sb}^m$  and  $^{122}\text{Sb}$  are given in Table 3.4 as taken from the NuDat 2.8 database [8].

**Table 3.4** Nuclear spectroscopic decay data half-lives, decay mode,  $\gamma$ -ray energies, intensities of the most intense  $\gamma$ -rays and reaction thresholds for samples and reference reactions with their uncertainties [8].

Reactions	$E_{th}$ (MeV)	Half-life ( $\tau_{1/2}$ )	Decay mode	$E_\gamma$ (keV)	$I_\gamma$ (%)
$^{121}\text{Sb}(n, 2n)^{120}\text{Sb}^m$	9.33	5.76 (2) day	$\varepsilon$ (100 %)	1171.3	100
$^{123}\text{Sb}(n, 2n)^{122}\text{Sb}$	9.03	2.72 (2) day	$\beta^-$ (97.59%) $\varepsilon$ (2.41%)	564.12	70.68 (18)
$^{103}\text{Rh}(n, 2n)^{102}\text{Rh}^g$	9.41	207.3 (17) day	$\varepsilon$ (78 %) $\beta^-$ (22 %)	468.6	2.90 (20)
$^{103}\text{Rh}(n, 2n)^{102}\text{Rh}^m$	9.55	3.74 (10) year	$\varepsilon$ (99.77 %) $IT$ (0.23 %)	697.5 766.8 1112.8	44.0 (20) 34.0 (20) 19.0 (10)
$^{51}\text{V}(n, p)^{51}\text{Ti}$	1.72	5.76 (1) m	$\beta^-$ (100 %)	320.08	93.1 (4)
$^{65}\text{Cu}(n, p)^{65}\text{Ni}$	1.37	2.52 (5) h	$\beta^-$ (100 %)	1115.53	15.43 (13)
$^{76}\text{Se}(n, p)^{76}\text{As}$	2.21	26.24 (9) h	$\beta^-$ (100 %)	559.10	45 (2)

$^{77}\text{Se}(n, p)^{77}\text{As}$	0.0	38.83 (5) h	$\beta^-$ (100 %)	238.99	1.6 (24)
$^{78}\text{Se}(n, p)^{78}\text{As}$	3.47	90.7 (2) m	$\beta^-$ (100 %)	613.81	54 (6)
$^{80}\text{Se}(n, p)^{80}\text{As}$	4.82	15.2 (2) sec	$\beta^-$ (100 %)	666.14	42 (5)
$^{27}\text{Al}(n, \alpha)^{24}\text{Na}$	3.25	14.99 (12) h	$\beta^-$ (100 %)	1368.62	99.99 (15)

### 3.4 Measurements of the neutron activation cross sections

The activation cross sections of the  $(n, p)$  and  $(n, 2n)$  reactions were estimated for the  $^{51}\text{V}$ ,  $^{65}\text{Cu}$ ,  $^{76,77,78,80}\text{Se}$ ,  $^{103}\text{Rh}$ ,  $^{121}\text{Sb}$  and  $^{123}\text{Sb}$  isotopes relative to the reference  $^{27}\text{Al}(n, \alpha)^{24}\text{Na}$  monitor reaction using the standard activation equation given as:

$$\langle \sigma_r \rangle = \langle \sigma_m \rangle \left( \frac{C_r \lambda_r W t_m A M_r A b u_m \varepsilon_m I_m f_m}{C_m \lambda_m W t_r A M_m A b u_r \varepsilon_r I_r f_r} \right) \times \frac{(C_{attn} * C_{low} * C_g)_r}{(C_{attn} * C_{low} * C_g)_m} \quad (6)$$

Where  $r$  and  $m$  in subscript stand for sample and monitor reaction.  $\sigma$  is the reaction cross sections,  $C$  is the detected photo-peak counts of the  $\gamma$ -ray of the reaction products,  $\lambda$  is the decay constant,  $\varepsilon$  is the efficiency for characteristic  $\gamma$ -ray of radionuclide,  $I$  is the  $\gamma$ -ray abundance,  $Wt$  is the weight,  $Abu$  is the isotopic abundance,  $AM$  is the atomic mass,  $f$  is the time factor,  $C_{low}$  is the low energy background neutron correction factor,  $C_{attn}$  is the  $\gamma$ -ray self-attenuation correction factor,  $C_g$  is the geometry correction factor. The timing factor as specified in equation (6) is given as:

$$f = (1 - \exp(-\lambda t_i)) \exp(-\lambda t_c) (1 - \exp(-\lambda t_m)) \quad (7)$$

Where,  $t_i$  is irradiation time,  $t_c$  is cooling time and  $t_m$  is counting time. The uncertainty in the time factor  $f$  is given by:

$$\left( \frac{\Delta f}{f} \right)^2 = \left( \frac{\lambda t_{irr} * \exp(-\lambda t_{irr})}{(1 - \exp(-\lambda t_{irr}))} - \lambda t_{cool} + \frac{\lambda t_{count} * \exp(-\lambda t_{count})}{(1 - \exp(-\lambda t_{count}))} - 1 \right)^2 \left( \frac{\Delta \lambda}{\lambda} \right)^2 \quad (8)$$

The present measured experimental results for the  $^{51}\text{V}(n, p)^{51}\text{Ti}$ ,  $^{65}\text{Cu}(n, p)^{65}\text{Ni}$ ,  $^{76}\text{Se}(n, p)^{76}\text{As}$ ,  $^{77}\text{Se}(n, p)^{77}\text{As}$ ,  $^{78}\text{Se}(n, p)^{78}\text{As}$ ,  $^{80}\text{Se}(n, p)^{80}\text{As}$ ,  $^{103}\text{Rh}(n, 2n)^{102}\text{Rh}$ ,  $^{103}\text{Rh}(n, 2n)^{102}\text{Rh}^m$ ,  $^{103}\text{Rh}(n, 2n)^{102}\text{Rh}^g$ ,  $^{121}\text{Sb}(n, 2n)^{120}\text{Sb}^m$  and  $^{123}\text{Sb}(n, 2n)^{122}\text{Sb}$  reactions cross sections relative to the reference  $^{27}\text{Al}(n, \alpha)^{24}\text{Na}$  monitor reaction using the standard activation and off-line  $\gamma$ -ray spectroscopy are given in Tables 3.5, 3.6, 3.7, 3.8 and 3.9.

**Table 3.5** The measured  $^{121}\text{Sb}(n, 2n)^{120}\text{Sb}^m$  and  $^{123}\text{Sb}(n, 2n)^{122}\text{Sb}$  reaction cross sections with their uncertainties at different energies.

$\langle E_n \rangle$ (MeV)	$^{121}\text{Sb}(n, 2n)^{120}\text{Sb}^m$ (mb)	$^{123}\text{Sb}(n, 2n)^{122}\text{Sb}$ (mb)
12.50±0.68	424.47±46.35	1371.74±130.56
15.79±0.55	596.25±94.37	1570.29±233.34
18.87±0.59	633.68±55.17	1412.50±101.63

**Table 3.6** The measured  $^{103}\text{Rh}(n, 2n)^{102}\text{Rh}$ ,  $^{103}\text{Rh}(n, 2n)^{102}\text{Rh}^m$  and  $^{103}\text{Rh}(n, 2n)^{102}\text{Rh}^g$  reactions cross sections with their uncertainties at two energies.

$\langle E_n \rangle \pm \Delta E_n$ (MeV)	$^{103}\text{Rh}(n, 2n)^{102}\text{Rh}^m$ (mb)	$^{103}\text{Rh}(n, 2n)^{102}\text{Rh}^g$ (mb)	$^{103}\text{Rh}(n, 2n)^{102}\text{Rh}$ (mb)	Ratio ( $\sigma_m/\sigma_g$ )
16.86±0.55	745.68±80.64	736.07±50.93	1481.75±131.57	1.013
19.89±0.59	588.74±63.04	446.73±41.21	1035.47±104.25	1.318

**Table 3.7** The measured  $^{51}\text{V}(n, p)^{51}\text{Ti}$  reaction cross sections with their uncertainties at different energies.

$\langle E_n \rangle$ (MeV)	$^{51}\text{V}(n, p)^{51}\text{Ti}$ (mb)
7.87 (58)	11.5 (27)
13.05 (68)	29.7 (35)
16.98 (53)	26.7 (39)

**Table 3.8** The measured  $(n, p)$  reaction cross sections for Se isotopes with their uncertainties at different energies.

$\langle E_n \rangle$ MeV	$^{76}\text{Se}(n, p)^{76}\text{As}$ (mb)	$^{77}\text{Se}(n, p)^{77}\text{As}$ (mb)	$^{78}\text{Se}(n, p)^{78}\text{As}$ (mb)	$^{80}\text{Se}(n, p)^{80}\text{As}$ (mb)
10.50±0.68	27.31±1.82	-	3.19±0.34	-
13.52±0.67	54.52±3.68	50.87±5.11	17.18±1.13	11.77±2.26
16.86±0.55	43.39±2.92	44.55±4.31	19.87±1.38	21.93±2.79
19.89±0.59	38.28±2.04	42.06±2.98	21.91±1.54	22.05±1.37

**Table 3.9** The measured  $^{65}\text{Cu}(n, p)^{65}\text{Ni}$  reaction cross sections with their uncertainties at different energies.

$\langle E_n \rangle \pm \Delta E_n$ (MeV)	$^{65}\text{Cu}(n, p)^{65}\text{Ni}$ (mb)
13.52±0.67	22.24±2.86
16.86±0.55	14.56±2.66
19.89±0.59	12.61±2.71

### 3.4.1 Reference cross section

The reference cross sections  $\langle\sigma_m\rangle$  of the monitor reaction  $^{27}\text{Al}(n,\alpha)^{24}\text{Na}$  were obtained using International Reactor Dosimetry and Fusion File (IRDFF-1.05) [9] database with the neutron flux energy spectrum. The  $^{27}\text{Al}(n,\alpha)^{24}\text{Na}$  reaction cross section known with an accuracy of 0.4 – 0.8% was used for the neutron fluence determination as to the reference data. The cross section data for the  $^{27}\text{Al}(n,\alpha)^{24}\text{Na}$  monitor reaction is shown in Fig. 3.7. This spectrum averaged cross sections were  $\langle\sigma_m\rangle$  obtained by the following relation:

$$\langle\sigma_m\rangle = \frac{\sum \varphi_0 \sigma_m(E) dE}{\sum \varphi_0 dE} \quad (9)$$

This spectrum averaged cross sections at  $10.50\pm 0.68$ ,  $13.52\pm 0.67$ ,  $16.86\pm 0.55$  and  $19.81\pm 0.59$  MeV neutron energies are as follows:  $94.36\pm 0.98$ ,  $125.45\pm 0.53$ ,  $100.79\pm 0.78$ ,  $44.03\pm 1.31$  (mb). Similarly, the spectrum averaged cross section covariance matrix at other different neutron energies is obtained by the IAEA neutron cross section standards IRDFF-1.05 database. The correlation coefficients are calculated using the following equation:

$$\text{Cor}(\langle\sigma_i\rangle\langle\sigma_j\rangle) = \text{Cov}(\langle\sigma_i\rangle\langle\sigma_j\rangle) / (\text{Var}\langle\sigma_i\rangle \cdot \text{Var}\langle\sigma_j\rangle)^{1/2} \quad (10)$$

The calculated spectrum averaged cross sections with their uncertainties and covariance and correlation matrix are given in Tables 3.10 and 3.11.

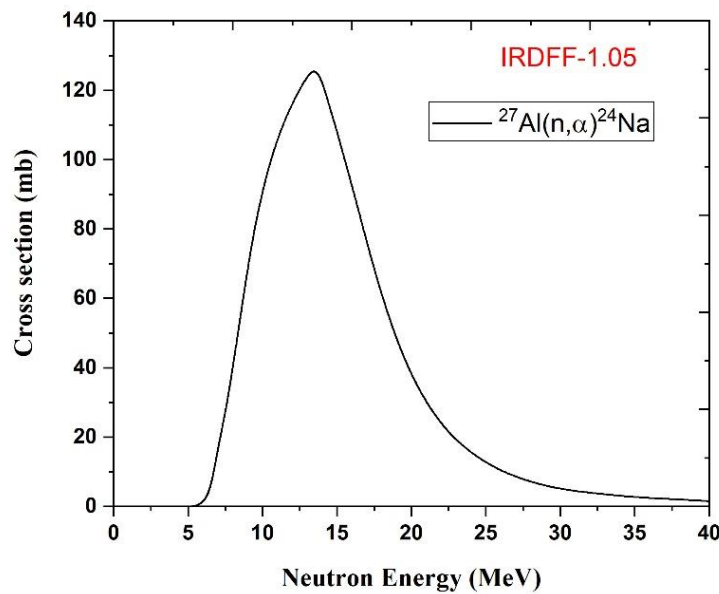


*Fig. 3.7 The standard IRDFF-1.05 data for the  $^{27}\text{Al}(n,\alpha)^{24}\text{Na}$  monitor reaction.*

**Table 3.10** The standard  $^{27}\text{Al}(n, \alpha)^{24}\text{Na}$  reaction cross section with their covariance and correlation matrix obtained from the IRDFF-1.05 database.

$\langle E_n \rangle$ (MeV)	Cross section (mb)	Covariance matrix			Correlation matrix		
12.50±0.68	118.94±0.079	0.006326			1.0		
15.79±0.55	114.38±0.067	0.000389	0.004493		0.0729	1.0	
18.87±0.59	55.74±0.108	0.002165	0.000917	0.01168	0.2517	0.1265	1.0

**Table 3.11** The standard  $^{27}\text{Al}(n, \alpha)^{24}\text{Na}$  reaction cross section with their covariance and correlation matrix obtained from the IRDFF-1.05 database.

$\langle E_n \rangle$ (MeV)	Cross section (mb)	Covariance matrix			Correlation matrix		
7.87±0.58	41.3±0.094	0.00875			1.0		
13.05±0.68	119.5±0.025	0.000791	0.000633		0.106	1.0	
16.98±0.53	80.8±0.083	0.00028	0.001334	0.00684	0.036	0.202	1.0

### 3.4.2 Estimation of the correction factors

The interaction of the  $\gamma$ -rays with materials requires the correction of the self-attenuation effect. Beer-Lambert's law gives a correction factor for the  $\gamma$ -ray self-attenuation factor  $\Gamma_{attn}$  for activated materials, which was calculated by the following relation  $C_{attn} = (1 - e^{-\mu l})/(\mu l)$  where  $l$  is the thickness of the materials and  $\mu$  is the mass attenuation coefficient of the  $\gamma$ -ray energy and material, which was calculated from the XMuDat ver.1.0.1 database [10]. The correction factor for the counting geometry is given as follow:

$$C_g = (D + h/2)^2 / D^2 \quad (11)$$

Where,  $h$  is the thickness of the sample and  $D$  is the distance from the measured sample to the surface of the Ge crystal. The  $(n, p)$  and  $(n, 2n)$  reactions cross sections were measured for the primary neutron energy peak as shown in Fig. 3.1. The spectral indexing method correction for low energy background neutron subtraction is given in Ref. [5] and the following relation subtracted the correction for the low energy background neutrons:

$$C_{low} = 1 - \frac{\int \phi(E_{p_1}) \sigma_i(E_{p_1})}{\int \phi(E) \sigma_i(E) dE} \quad (12)$$

Where  $E_{p_1}$  and  $E_{p_2}$  are primary and secondary neutron energy peaks in the neutron flux spectrum,  $\phi(E) = \phi(E_{p_1}) + \phi(E_{p_2})$  is the neutron flux, and  $\sigma_i(E)$  is the reaction cross sections. The cross section  $\sigma_i(E)$  of the sample reaction was taken from the evaluated data of the ENDF/B-VIII.0 [11] library and for the  $^{27}\text{Al}(n, \alpha)^{24}\text{Na}$  reference reaction was taken from the IRDFF-1.05 library. This IRDFF-1.05 library seems to be most preferable for this purpose because this evaluation is one of the latest and contains detailed information on both cross sections and uncertainties. The correction factors used in the cross section calculation are given in Table 3.12.

**Table 3.12** The values of  $\gamma$ -ray self-attenuation and low energy background neutrons correction factors used to measure the cross section.

Reactions	$\langle E_n \rangle$ MeV	$E_\gamma$ (keV)	$(C_{\text{attn}})$	$(C_{\text{low}})$	$(C_g)$
$^{121}\text{Sb}(n, 2n)^{120}\text{Sb}^{\text{m}}$	12.50		0.988029	0.99948	1.0235
	15.79	1171.2	0.988064	0.96515	
	18.87		0.988076	0.90076	
$^{123}\text{Sb}(n, 2n)^{122}\text{Sb}$	12.50		0.980661	0.99841	1.0235
	15.79	564.2	0.980717	0.95577	
	18.87		0.980736	0.88616	
$^{27}\text{Al}(n, \alpha)^{24}\text{Na}$	12.50		0.999322	0.87381	1.0033
	15.79	1368.62	0.999330	0.90274	
	18.87		0.999320	0.75953	
$^{103}\text{Rh}(n, 2n)^{102}\text{Rh}^{\text{m}}$	16.86	697.5	0.98275	0.9251	1.0094
	19.81	766.8	0.98182	0.9016	1.0099
$^{103}\text{Rh}(n, 2n)^{102}\text{Rh}^{\text{g}}$	16.86		0.98275	0.9251	1.0094
	19.81	468.6	0.98182	0.9016	1.0099
$^{76}\text{Se}(n, p)^{76}\text{As}$ $^{77}\text{Se}(n, p)^{77}\text{As}$ $^{78}\text{Se}(n, p)^{78}\text{As}$ $^{80}\text{Se}(n, p)^{80}\text{As}$	10.50	559.1	0.992678	3.711	1.0269
		238.9	0.985129	2.315	1.0280
		613.8	0.992888	2.767	1.0267
		666.2	0.993310	3.224	1.0295
	13.52	559.1	0.992384	3.618	1.0269
		238.9	0.984536	2.284	1.0280
		613.8	0.992602	2.646	1.0267
		666.2	0.993042	3.020	1.0295
	16.86	559.1	0.992726	2.504	1.0269
		238.9	0.985227	2.087	1.0280
		613.8	0.992935	2.314	1.0267
		666.2	0.993354	2.676	1.0295
	19.81	559.1	0.991978	2.114	1.0269
		238.9	0.983716	2.018	1.0280
		613.8	0.992208	2.123	1.0267
		666.2	0.992671	2.360	1.0295

$^{27}\text{Al}(n, \alpha)^{24}\text{Na}$	10.50	1368.62	0.999106	3.535	1.0032
	13.52		0.999254	2.491	1.0034
	16.86		0.999174	2.313	1.0038
	19.81		0.999165	2.868	1.0039
$^{51}\text{V}(n, p)^{51}\text{Ti}$	7.87	320.08	0.981029	0.68245	1.0207
	13.05		0.981003	0.81394	
	16.98		0.981022	0.89084	
$^{27}\text{Al}(n, \alpha)^{24}\text{Na}$	7.87	1368.62	0.999322	0.96768	1.0033
	13.05		0.999317	0.87381	
	16.98		0.999320	0.86452	
$^{65}\text{Cu}(n, p)^{65}\text{Ni}$	13.52	1115.53	0.99202	0.7377	1.0107
	16.86		0.99071	0.8668	1.0124
	19.81		0.99088	0.8167	1.0122

### 3.5 Uncertainties in the data and covariance analysis

The cross sections were calculated using the activation method relative to the  $^{27}\text{Al}(n, \alpha)^{24}\text{Na}$  reference reaction and the uncertainties in the measured cross sections arise from the counting statistics of the detected photo-peak counts of the  $\gamma$ -rays of the reaction products of both the samples and the aluminium monitor. The other uncertainties associated with the measured cross sections include uncertainties in (i) monitor cross sections (ii) detector efficiency (iii)  $\gamma$ -ray self-absorption (iv) atomic mass (v) decay data (vi) weight (vii) time factor (viii) isotopic abundance. The cross section uncertainties were calculated by taking the square root of the quadratic sum of all the individual uncertainties for Rh and Cu nuclei, whereas by the covariance method for the Sb, V and Se nuclei as mentioned in the section 3.5.1. The error propagation expression for the measured cross section is written in ref. [12].

The uncertainties in the measured  $^{103}\text{Rh}(n, 2n)^{102}\text{Rh}^m$  and  $^{103}\text{Rh}(n, 2n)^{102}\text{Rh}^g$  reactions cross sections cross section at two different energies were calculated by taking the square root of the quadratic sum of all the individual uncertainties involved in all parameters. The uncertainties in the isotopic abundance, atomic mass, half-life and  $\gamma$ -ray abundances were taken from the National Nuclear data Center (NNDC) database. The uncertainties of different parameters contribute to the total uncertainty of the measured cross section. The source of uncertainty in the measured cross section and their values are listed below: Decay data (< 0.35) %, counts of  $\gamma$ -peak (< 9) %, the efficiency of  $\gamma$ -detector (< 2.5) %, corrections for self-absorption,  $\gamma$ -cascade summing (< 0.5) %, reference cross sections used for neutron fluence determination (< 1%), sample mass (< 0.1) %, isotopic abundance (< 1.0%). The contribution of uncertainties of other parameters is very small and can be neglected. As can be seen, the

uncertainty of the  $^{103}\text{Rh}(n, 2n)^{102}\text{Rh}^{\text{m}}$ , and  $^{103}\text{Rh}(n, 2n)^{102}\text{Rh}^{\text{g}}$  reactions cross sections are in range of 7 to 11 %.

Similarly, the uncertainties in the measured  $^{65}\text{Cu}(n, p)^{65}\text{Ni}$  reaction cross sections arise from the counting statistics of the detected photo-peak counts of the  $\gamma$ -rays of the reaction products of both the copper sample and the aluminium monitor. The uncertainties associated with the measured cross sections include uncertainties in (i) monitor cross sections (ii) counting statistics (iii) detector efficiency (iv)  $\gamma$ -ray self-absorption (v) atomic mass (vi) decay data (vii) weight (viii) isotopic abundance and (ix) time factor. Total uncertainties were estimated in quadrature by taking the square root of the sum of the squares of the individual uncertainties. The compilation of the uncertainties for the measured  $^{65}\text{Cu}(n, p)^{65}\text{Ni}$  reaction cross section are mentioned in Table 3.13.

**Table 3.13** Compilation of the uncertainties (%) for the measured  $^{65}\text{Cu}(n, p)^{65}\text{Ni}$  reaction cross section.

Uncertainties	Sample (Cu)	Monitor reaction (Al)
Monitor cross section	-	0.2-0.5
Counting statistics	15	5
Detector efficiency	2	1.43
$\gamma$ -ray self-absorption	<1	<1
Atomic mass	0.008	0.01
Half-life	0.02	0.08
Weight	0.02	0.02
Abundance	0.09	-
$\gamma$ -ray intensity	0.84	0.15
time factor	0.5	0.5

### 3.5.1 Covariance analysis

We calculated the covariance matrix for the detector efficiency and reaction cross section in the above data analysis. All the uncertainty information for the experimental data is included in the covariance matrix. Therefore, the calculated matrix gives complete information of the uncertainties in the measured efficiency and cross sections. The efficiencies of the detector were measured using  $\gamma$ -lines of the calibrated  $^{152}\text{Eu}$  point source. The following relation was used to estimate the efficiency of the HPGe detector:

$$\varepsilon = \frac{CK_c}{N_0 I_\gamma e^{-\lambda t}} \quad (13)$$

where  $\varepsilon$  is the efficiency of the corresponding  $\gamma$ -rays,  $C$  is the count under gamma peak,  $N_0$  activity of standard  $^{152}\text{Eu}$  source at an initial time ( $7767.73 \pm 88.13$  Bq),  $I_\gamma$  is the  $\gamma$ -ray intensity,  $\lambda$  is the decay constant of  $^{152}\text{Eu}$ , and  $K_c$  is the correction factor for the coincidence summing effect,  $t$  is the time elapsed from the manufacturer date to the start of counting. The correction factor  $K_c$  was calculated from the Monte Carlo Simulation code EFFTRAN [13] using HPGe detector structured data such as crystal hole cavity, end cup, mount cup, crystal material, dimension, absorber, window and calibration source information. It is observed that the HPGe detector efficiency is the function of counts, decay constant, the activity of source and  $\gamma$ -ray intensity. The uncertainty for the  $\gamma$ -ray intensity and half-life for  $^{152}\text{Eu}$  source were taken from NNDC nuclear database and uncertainty in these four variables propagates in the detector efficiency estimation. Therefore, detector efficiency can be written as the function of only four attributes, such as  $I_\gamma, \lambda, C, N_0$ . The total uncertainties due to four attributes in detector efficiency were calculated using quadratic sum formula:

$$\left(\frac{\Delta\varepsilon_i}{\varepsilon_i}\right)^2 = \left(\frac{\Delta C_i}{C_i}\right)^2 + \left(\frac{\Delta I_{\gamma i}}{I_{\gamma i}}\right)^2 + \left(\frac{\Delta N_0}{N_0}\right)^2 + (t\Delta\lambda)^2 \quad (14)$$

Uncertainty in the decay constant is  $\Delta\lambda = (0.693 * \Delta\tau_{1/2} / \tau_{1/2}^2)$ .

The partial uncertainties of various parameters of the HPGe detector efficiency for two different irradiations obtained from equation (14) are mentioned in Tables 3.14 and 3.15.

**Table 3.14** The partial uncertainties of various parameters used to obtain HPGe detector efficiency (Sb and V data).

$E_\gamma$ (keV)	Counts ( $\times 10^{-4}$ )	Half-life ( $\tau_{1/2}$ ) ( $\times 10^{-4}$ )	$I_\gamma$ ( $\times 10^{-4}$ )	Activity ( $N_0$ ) ( $\times 10^{-4}$ )	Total Uncertainty ( $\times 10^{-4}$ )
121.78	0.619	2.092	1.331	2.698	3.716
244.69	1.081	1.556	4.434	2.008	5.223
344.27	0.489	1.166	2.001	1.504	2.804
443.96	1.455	1.105	0.623	1.426	2.401
778.91	0.457	0.522	3.665	0.673	3.791
964.08	0.391	0.433	2.359	0.558	2.493
1085.86	0.381	0.358	1.995	0.462	2.114
1408.01	0.261	0.285	1.389	0.368	1.488

**Table 3.15** The partial uncertainties in the HPGe detector efficiency due to the different attributes (Se data).

$E_\gamma$ (keV)	$I_\gamma$ ( $\times 10^{-4}$ )	Counts ( $\times 10^{-4}$ )	Activity ( $N_0$ ) ( $\times 10^{-4}$ )	Half-life ( $\tau_{1/2}$ ) ( $\times 10^{-4}$ )	Total Uncertainty ( $\times 10^{-4}$ )
121.78	1.459	1.597	7.884	2.329	2.863
244.69	8.470	2.002	3.836	1.133	1.479
344.27	3.770	8.923	2.833	8.369	9.648
443.96	4.392	2.195	2.008	5.932	7.958
778.91	1.259	0.695	0.973	2.874	3.358
964.08	1.024	0.627	0.808	2.387	2.792
1085.87	1.276	0.623	0.703	2.079	2.614
1299.14	0.925	1.501	0.568	1.678	2.499
1408.01	0.465	0.386	0.462	1.365	1.563

The knowledge about the partial uncertainties and their correlations provides a foundation for creating the covariance matrix, which fully describes the uncertainties in the calculated efficiencies. It is possible to directly calculate the elements of this covariance matrix using the formula:

$$(V_\varepsilon)_{ij} = \sum_r e_{ir} S_{ijr} e_{jr} \quad (15)$$

Where  $S_{ijr}$  is the  $n \times n$  micro-correlation matrix between the  $i^{th}$  and  $j^{th}$  observations due to the  $r^{th}$  attributes,  $e_{ir}$  and  $e_{jr}$  is the  $n \times n$  diagonal matrix of partial uncertainties  $i^{th}$  and  $j^{th}$  observations due to the  $r^{th}$  attributes [14]. The total error in the measured efficiencies is related to the variances by the formula  $\sigma_{\varepsilon ii} = ((V_\varepsilon)_{ii})^{1/2}$ . The calculated covariance and correlation matrix for the HPGe detector efficiency is given in Tables 3.16 and 3.17.

**Table 3.16** The calculated covariance and correlation matrix for the HPGe detector efficiencies (Sb and V).

$E_\gamma$ (keV)	Covariance matrix ( $\times 10^{-8}$ )	Correlation matrix
121.78	13.81	1.0
244.69	8.672 27.28	0.446 1.0
344.27	6.497 4.834 7.865	0.623 0.331 1.0
443.96	6.159 4.852 3.433 5.761	0.691 0.365 0.511 1.0
778.91	2.906 2.162 1.619 1.535 14.36	0.206 0.109 0.152 0.168 1.0
964.08	2.411 1.794 1.344 1.274 0.601 6.216	0.261 0.137 0.192 0.213 0.063 1.0
1085.86	1.966 1.485 1.112 1.054 0.497 0.413 4.466	0.254 0.134 0.187 0.208 0.062 0.078 1.0
1408.01	1.588 1.182 0.885 0.839 0.396 0.328 0.272 2.214	0.287 0.152 0.212 0.235 0.071 0.089 0.086 1.0

**Table 3.17** The calculated covariance and correlation matrix for the HPGe detector efficiencies (Se data).

$E_\gamma$ (keV)	Covariance matrix ( $\times 10^{-8}$ )	Correlation matrix
121.78	820.1	1.0
244.69	294.1 218.8	0.694 1.0
344.27	217.2 105.6 93.08	0.786 0.741 1.0
443.96	153.9 74.91 55.33 63.32	0.675 0.636 0.721 1.0
778.91	74.61 36.29 26.81 19.01 11.27	0.776 0.731 0.827 0.711 1.0
964.08	61.96 30.14 22.26 15.78 7.646 7.793	0.775 0.730 0.826 0.710 0.815 1.0
1085.86	53.96 26.25 19.39 13.74 6.659 5.531 6.833	0.721 0.678 0.768 0.660 0.758 0.757 1.0
1299.14	43.55 21.19 15.65 11.09 5.375 4.464 3.888 6.274	0.608 0.573 0.649 0.557 0.641 0.639 0.595 1.0
1408.01	35.43 17.23 12.73 9.025 4.372 3.631 3.163 2.552 2.418	0.792 0.745 0.844 0.725 0.833 0.832 0.774 0.653 1.0

The  $\gamma$ -rays emitted by  $^{51}\text{Ti}$ ,  $^{76}\text{As}$ ,  $^{77}\text{As}$ ,  $^{78}\text{As}$ ,  $^{80}\text{As}$ ,  $^{120}\text{Sb}^m$ ,  $^{122}\text{Sb}$  and  $^{24}\text{Na}$  nuclei are different from the  $\gamma$ -ray of standard  $^{152}\text{Eu}$  source. A linear interpolation method was used in the calculation to estimate efficiencies for the corresponding  $\gamma$ -rays of  $^{51}\text{Ti}$ ,  $^{76}\text{As}$ ,  $^{77}\text{As}$ ,  $^{78}\text{As}$ ,  $^{80}\text{As}$ ,  $^{120}\text{Sb}^m$ ,  $^{122}\text{Sb}$  and  $^{24}\text{Na}$  nuclei. An empirical relation as a model through interpolation using the following linear parametric function:

$$\ln(\varepsilon_i) = \sum_{k=1}^m p_k (\ln[E_i])^{k-1} \quad (16)$$

Where  $\varepsilon_i$  is the efficiency for the corresponding  $\gamma$ -ray energy,  $E_i$  and  $p_k$  is the fitting parameter. The least-square condition states that the best estimate for  $\hat{P}$  in the model is the one that minimizes the chi-square statistic given by  $\chi_m^2 = (Z - AP)' V_Z^{-1} (Z - AP)$ . From the least square method, the best estimate  $\hat{P}$  calculated by the following relation:

$$\hat{P} = (A^T V_Z^{-1} A)^{-1} (A^T V_Z^{-1} Z) \quad (17)$$

In the above equation  $\hat{P}$  is the column matrix,  $V_Z$  was calculated as  $(V_\varepsilon)_{ij} / \varepsilon_i \varepsilon_j$  where  $V_\varepsilon$  is the covariance matrix for the corresponding efficiencies  $\varepsilon$ ,  $A$  is the design matrix with  $A_{ik} = (\ln[E_i])^{k-1}$ ,  $k = 1, 2, \dots, 7$ ,  $i = 1, 2, \dots, 8$  and  $Z$  is the column matrix with  $Z_i = \ln(\varepsilon_i)$  [15]. The best fit of the chosen model in the present work was obtained by considering six parameters and the model gives the best fit value for  $k=7$  and  $i=8$ , with the goodness of fit  $\chi^2 = 0.799$ . We consider the following linear parametric model as the best model, which gives the values of fitting parameters  $\hat{P} = -5.453, -1.092, 1.783, -0.0567, -5.579, -4.976, -1.208$ . From the above calculation, the correlation matrix and efficiencies for the characteristics  $\gamma$ -rays of the  $^{51}\text{Ti}$ ,  $^{120}\text{Sb}^m$ ,  $^{122}\text{Sb}$  and  $^{24}\text{Na}$  are given in Tables 3.18 and 3.19.

**Table 3.18** The interpolated detector efficiencies of the characteristics  $\gamma$ -ray of the  $^{51}\text{Ti}$  and  $^{24}\text{Na}$  product nuclide with their uncertainties along with covariance and correlation matrix.

Reaction	$E_\gamma$ (keV)	Efficiency	Covariance Matrix ( $\times 10^{-8}$ )	Correlation matrix
$^{51}\text{V}(n, p)^{51}\text{Ti}$	302.08	0.0135 (0.031)	9.791	1.0
$^{27}\text{Al}(n, \alpha)^{24}\text{Na}$	1368.62	0.0034 (0.014)	0.743 1.929	0.172 1.0

**Table 3.19** The interpolated detector efficiencies of the characteristics  $\gamma$ -ray of the  $^{120}\text{Sb}^m$ ,  $^{122}\text{Sb}$  and  $^{24}\text{Na}$  product nuclide with their uncertainties along with covariance and correlation matrix.

Reaction	$E_\gamma$ (keV)	Efficiency	Covariance Matrix ( $\times 10^{-8}$ )	Correlation matrix
$^{121}\text{Sb}(n, 2n)^{120}\text{Sb}^m$	1171.2	0.00375 $\pm$ 0.000133	1.764	1.0
$^{123}\text{Sb}(n, 2n)^{122}\text{Sb}$	564.2	0.01079 $\pm$ 0.000299	1.913 8.931	0.4826 1.0
$^{27}\text{Al}(n, \alpha)^{24}\text{Na}$	1368.6	0.00337 $\pm$ 0.000139	1.187 0.4376 1.929	0.6459 0.1056 1.0

Similarly, the best fit of the chosen model in the present work for the selenium data was obtained by considering six parameters and the model is given the best fit value for  $k=6$  and  $i=9$ , with the goodness of fit  $\chi^2 = 1.179$ . We consider the following linear parametric model as the optimum model, which gives the value of fitting parameters as follows:  $\hat{P} = -4.98363, -0.935804, -0.591703, -2.43244, -2.07165, -0.507021$ . The correlation matrix and efficiencies for the characteristics  $\gamma$ -ray of the  $^{76}\text{As}$ ,  $^{77}\text{As}$ ,  $^{78}\text{As}$ ,  $^{80}\text{As}$  and  $^{24}\text{Na}$  product nuclide are given in Table 3.20.

**Table 3.20** The interpolated detector efficiencies of the characteristics  $\gamma$ -ray of the  $^{76}\text{As}$ ,  $^{77}\text{As}$ ,  $^{78}\text{As}$ ,  $^{80}\text{As}$  and  $^{24}\text{Na}$  product nuclide with their uncertainties along with covariance and correlation matrix.

Reactions	$E_\gamma$ (keV)	Efficiency	Covariance Matrix ( $\times 10^{-7}$ )	Correlation matrix
$^{76}\text{Se}(n, p)^{76}\text{As}$	559.1	0.012721 $\pm$ 0.000518	2.687	1.0
$^{77}\text{Se}(n, p)^{77}\text{As}$	238.9	0.034296 $\pm$ 0.001534	5.156 23.35	0.6484 1.0
$^{78}\text{Se}(n, p)^{78}\text{As}$	613.8	0.011237 $\pm$ 0.000459	2.375 4.715 2.115	0.9966 0.6683 1.0
$^{80}\text{Se}(n, p)^{80}\text{As}$	666.2	0.010165 $\pm$ 0.000412	2.111 4.378 1.888 1.695	0.9893 0.6933 0.9976 1.0
$^{27}\text{Al}(n, \alpha)^{24}\text{Na}$	1368.6	0.004373 $\pm$ 0.000164	0.673 1.849 0.592 0.535 0.268	0.7928 0.7363 0.7859 0.7943 1.0

In covariance analysis, a ratio method was used for the calculation of activation cross section. In the standard activation equation (6), the sample reaction cross section was normalized to the monitor  $^{27}\text{Al}(n, \alpha)^{24}\text{Na}$  reaction cross section. We got the ratio of  $\langle \sigma_r \rangle$  and  $\langle \sigma_m \rangle$  i.e., the sample and monitor reaction cross section. The covariance matrix for the measured cross section was calculated by the following formula:

$$(V_{\sigma_s})_{ij} = \sum_r e_{ir} S_{ijr} e_{jr} \quad (18)$$

Where  $S_{ijr}$  is the  $n \times n$  micro-correlation matrix between the  $i^{\text{th}}$  and  $j^{\text{th}}$  observations due to the  $r^{\text{th}}$  attributes,  $e_{ir}$  and  $e_{jr}$  are the  $n \times n$  diagonal matrix of partial uncertainty  $i^{\text{th}}$  and  $j^{\text{th}}$  observations due to the  $r^{\text{th}}$  attributes.

The Table 3.21 summarizes the partial uncertainties in various parameters to obtain  $(n, 2n)$  reaction cross section of Sb isotopes. The calculated covariance and correlation matrix for the  $^{121}\text{Sb}(n, 2n)^{120}\text{Sb}^m$  and  $^{123}\text{Sb}(n, 2n)^{122}\text{Sb}$  reactions cross sections is given in Table 3.22. The error in the measured cross sections are calculated by taking the square root of the diagonal elements of the covariance matrix i.e.  $((V_{\sigma_s})_{ii})^{1/2}$ . The source of uncertainty and their values in the present measured cross sections are given as follows: counting statistics ( $\leq 5\%$ ), isotopic abundance ( $\leq 1\%$ ), detector efficiency ( $\leq 4\%$ ), the weight of samples ( $\leq 0.01\%$ ), reference cross section ( $\leq 1\%$ ), and self-absorption of  $\gamma$ -ray ( $\leq 1\%$ ). The uncertainties due to the other sources are very small and neglected in measured  $^{121}\text{Sb}(n, 2n)^{120}\text{Sb}^m$  and  $^{123}\text{Sb}(n, 2n)^{122}\text{Sb}$  reactions cross sections.

**Table 3.21** The partial uncertainties in various parameters to obtain the  $^{121}\text{Sb}(n, 2n)^{120}\text{Sb}^m$  and  $^{123}\text{Sb}(n, 2n)^{122}\text{Sb}$  reactions cross section.

Parameters	$^{121}\text{Sb}(n, 2n)^{120}\text{Sb}^m$			$^{123}\text{Sb}(n, 2n)^{122}\text{Sb}$		
	$\langle E_n \rangle = 12.50$ (MeV)	$\langle E_n \rangle = 15.79$ (MeV)	$\langle E_n \rangle = 18.87$ (MeV)	$\langle E_n \rangle = 12.50$ (MeV)	$\langle E_n \rangle = 15.79$ (MeV)	$\langle E_n \rangle = 18.87$ (MeV)
$\sigma_{Al}$	2.838	3.498	12.289	9.172	9.218	2.740
$C_{Sb}$	22.657	32.923	17.691	23.466	28.323	15.095
$AM_{Sb}$	0.070	0.099	0.105	0.112	0.128	0.115
$\lambda_{Sb}$	2.963	4.232	5.993	9.353	10.802	9.289
$W_{Al}$	6.367	11.925	15.842	27.435	39.282	3.533
$I\gamma_{Al}$	0.170	0.239	0.253	0.549	0.629	0.565
$\epsilon_{Al}$	17.450	24.512	26.051	56.392	64.596	58.090
$C_{Al}$	31.208	77.626	31.804	100.852	204.565	70.918

$AM_{Al}$	0.472	0.663	0.705	1.525	1.747	1.571
$\lambda_{Al}$	1.117	2.063	3.128	3.608	5.438	6.684
$W_{Sb}$	8.504	23.850	9.505	27.480	62.852	2.120
$Abun_{Sb}$	0.212	0.298	0.317	0.683	0.782	0.703
$I\gamma_{Sb}$	0.006	0.009	0.010	2.465	2.823	2.539
$\varepsilon_{Sb}$	15.010	21.085	22.408	37.983	43.509	39.127

**Table 3.22** The calculated covariance and correlation matrix at 12.50, 15.79 and 18.87 MeV neutron energies for the  $^{121}\text{Sb}(n, 2n)^{120}\text{Sb}^m$  and  $^{123}\text{Sb}(n, 2n)^{122}\text{Sb}$  reactions cross section.

$\langle E_n \rangle$ (MeV)	Covariance matrix	Correlation matrix
12.50±0.68	2148.1 759.47 8905.3	1.0 0.1735 1.0
15.79±0.55	812.63 1332.3 3044.3 5140.8 2191.7 2332.7 17045.4	0.3176 0.2556 1.0 0.8483 0.1775 0.3233 1.0
18.87±0.59	1787.3 20391.8 3298.3 5426.4 54449.1 1609.3 2305.94 4777.9 4882.4 5741.1 10328.1	0.1652 0.9253 0.2561 0.1778 1.0 0.3412 0.2401 0.8511 0.3672 0.2418 1.0

Similarly, the covariance matrix for the  $\text{Se}(n, p)\text{As}$  reaction was calculated from equation (18) and Table 3.23 summarizes the partial uncertainties in various parameters to obtain  $(n, p)$  reaction cross section of Se isotopes. The calculated covariance and correlation matrix is given in Table 3.24. Different uncertainties involved in the cross sections measurement and the estimated error in different parameters are due to (i) detector efficiency (<3-4%), (ii) weight (<0.006%), (iii) counts (<3-5%), (iv) self-absorption of  $\gamma$ -ray (<0.4%), (v) reference cross section of  $^{27}\text{Al}(n, \alpha)^{24}\text{Na}$  reaction (<2-3%), (vi) absolute  $\gamma$ -ray intensity (<1%), (vii) Low energy background neutrons correction (<1%). The uncertainties in the measured cross sections for selenium were obtained by taking the square root of the diagonal elements of the covariance matrix.

**Table 3.23** The partial uncertainties in various parameters to obtain the  $(n, p)$  reaction cross section for Se isotopes.

$^{76}\text{Se}(n, p)^{76}\text{As}$				
Parameters	10.50 MeV	13.52 MeV	16.86 MeV	19.81 MeV
$\sigma_{Al}$	$3.00 \times 10^{-4}$	$5.42 \times 10^{-4}$	$4.76 \times 10^{-4}$	$3.82 \times 10^{-4}$
$C_{Se}$	$1.44 \times 10^{-3}$	$2.78 \times 10^{-3}$	$2.17 \times 10^{-3}$	$1.36 \times 10^{-3}$
$AM_{Se}$	$6.12 \times 10^{-9}$	$1.22 \times 10^{-8}$	$9.69 \times 10^{-9}$	$8.57 \times 10^{-9}$

$\lambda_{Se}$	$1.13 \times 10^{-4}$	$2.17 \times 10^{-4}$	$1.71 \times 10^{-4}$	$1.43 \times 10^{-4}$
$W_{Al}$	$2.73 \times 10^{-5}$	$5.63 \times 10^{-5}$	$4.04 \times 10^{-5}$	$3.53 \times 10^{-5}$
$I\gamma_{Al}$	$4.10 \times 10^{-5}$	$8.16 \times 10^{-5}$	$6.49 \times 10^{-5}$	$5.74 \times 10^{-5}$
$\varepsilon_{Al}$	$5.19 \times 10^{-4}$	$1.03 \times 10^{-3}$	$8.22 \times 10^{-4}$	$7.27 \times 10^{-4}$
$C_{Al}$	$6.76 \times 10^{-4}$	$1.70 \times 10^{-3}$	$1.38 \times 10^{-3}$	$9.30 \times 10^{-4}$
$AM_{Al}$	$5.06 \times 10^{-9}$	$1.01 \times 10^{-8}$	$8.02 \times 10^{-9}$	$7.09 \times 10^{-9}$
$\lambda_{Al}$	$1.48 \times 10^{-5}$	$1.92 \times 10^{-6}$	$2.66 \times 10^{-5}$	$1.29 \times 10^{-5}$
$W_{Se}$	$1.57 \times 10^{-6}$	$3.47 \times 10^{-6}$	$2.89 \times 10^{-6}$	$2.32 \times 10^{-6}$
$Abun_{Se}$	$3.21 \times 10^{-4}$	$6.39 \times 10^{-4}$	$5.08 \times 10^{-4}$	$4.50 \times 10^{-4}$
$I\gamma_{Se}$	$1.21 \times 10^{-4}$	$2.42 \times 10^{-4}$	$1.92 \times 10^{-4}$	$1.70 \times 10^{-4}$
$\varepsilon_{Se}$	$5.10 \times 10^{-4}$	1.02E-03	$8.08 \times 10^{-4}$	$7.15 \times 10^{-4}$
$C_{attn(Al)}$	$9.39 \times 10^{-5}$	$1.87 \times 10^{-4}$	$1.49 \times 10^{-4}$	$1.32 \times 10^{-4}$
$C_{attn(Se)}$	$8.48 \times 10^{-5}$	$1.69 \times 10^{-4}$	$1.34 \times 10^{-4}$	$1.19 \times 10^{-4}$
$^{77}\text{Se}(n, p)^{77}\text{As}$				
Parameters	13.52 MeV	16.86 MeV	19.81 MeV	
$\sigma_{Al}$	$5.06 \times 10^{-4}$	$4.89 \times 10^{-4}$	$4.20 \times 10^{-4}$	
$C_{Se}$	$4.58 \times 10^{-3}$	$3.81 \times 10^{-3}$	$2.45 \times 10^{-3}$	
$AM_{Se}$	$4.62 \times 10^{-9}$	$4.04 \times 10^{-9}$	$3.83 \times 10^{-9}$	
$\lambda_{Se}$	$5.78 \times 10^{-5}$	$5.10 \times 10^{-5}$	$5.05 \times 10^{-5}$	
$W_{Al}$	$5.25 \times 10^{-5}$	$4.15 \times 10^{-5}$	$3.88 \times 10^{-5}$	
$I\gamma_{Al}$	$7.62 \times 10^{-5}$	$6.67 \times 10^{-5}$	$6.31 \times 10^{-5}$	
$\varepsilon_{Al}$	$9.64 \times 10^{-4}$	$8.44 \times 10^{-4}$	$7.99 \times 10^{-4}$	
$C_{Al}$	$1.58 \times 10^{-3}$	$1.41 \times 10^{-3}$	$1.02 \times 10^{-3}$	
$AM_{Al}$	$9.41 \times 10^{-9}$	$8.23 \times 10^{-9}$	$7.79 \times 10^{-9}$	
$\lambda_{Al}$	$1.79 \times 10^{-6}$	$2.73 \times 10^{-5}$	$1.42 \times 10^{-5}$	
$W_{Se}$	$3.25 \times 10^{-6}$	$2.97 \times 10^{-6}$	$2.55 \times 10^{-6}$	
$Abun_{Se}$	$3.99 \times 10^{-4}$	$3.49 \times 10^{-4}$	$3.31 \times 10^{-4}$	
$I\gamma_{Se}$	$7.61 \times 10^{-4}$	$6.66 \times 10^{-4}$	$6.31 \times 10^{-4}$	
$\varepsilon_{Se}$	$8.18 \times 10^{-4}$	$7.16 \times 10^{-4}$	$6.78 \times 10^{-4}$	

$C_{attn(Al)}$	$1.75 \times 10^{-4}$	$1.53 \times 10^{-4}$	$1.45 \times 10^{-4}$	
$C_{attn(Se)}$	$1.58 \times 10^{-4}$	$1.38 \times 10^{-4}$	$1.31 \times 10^{-4}$	
$^{78}\text{Se}(n, p)^{78}\text{As}$				
Parameters	10.50 MeV	13.52 MeV	16.86 MeV	19.81 MeV
$\sigma_{Al}$	$3.50 \times 10^{-5}$	$1.71 \times 10^{-4}$	$2.18 \times 10^{-4}$	$2.19 \times 10^{-4}$
$C_{Se}$	$3.14 \times 10^{-4}$	$8.09 \times 10^{-4}$	$7.40 \times 10^{-4}$	$9.70 \times 10^{-4}$
$AM_{Se}$	$7.78 \times 10^{-10}$	$4.18 \times 10^{-9}$	$4.83 \times 10^{-9}$	$5.34 \times 10^{-9}$
$\lambda_{Se}$	$1.11 \times 10^{-6}$	$5.03 \times 10^{-6}$	$5.81 \times 10^{-6}$	$1.71 \times 10^{-5}$
$W_{Al}$	$3.19 \times 10^{-6}$	$1.77 \times 10^{-5}$	$1.85 \times 10^{-5}$	$2.02 \times 10^{-5}$
$I\gamma_{Al}$	$4.79 \times 10^{-6}$	$2.57 \times 10^{-5}$	$2.97 \times 10^{-5}$	$3.29 \times 10^{-5}$
$\varepsilon_{Al}$	$6.06 \times 10^{-5}$	$3.26 \times 10^{-4}$	$3.76 \times 10^{-4}$	$4.16 \times 10^{-4}$
$C_{Al}$	$7.90 \times 10^{-5}$	$5.34 \times 10^{-4}$	$6.31 \times 10^{-4}$	$5.33 \times 10^{-4}$
$AM_{Al}$	$5.91 \times 10^{-10}$	$3.18 \times 10^{-9}$	$3.67 \times 10^{-9}$	$4.06 \times 10^{-9}$
$\lambda_{Al}$	$1.72 \times 10^{-6}$	$6.04 \times 10^{-7}$	$1.22 \times 10^{-5}$	$7.38 \times 10^{-6}$
$W_{Se}$	$1.84 \times 10^{-7}$	$1.09 \times 10^{-6}$	$1.33 \times 10^{-6}$	$1.33 \times 10^{-6}$
$Abun_{Se}$	$1.21 \times 10^{-5}$	$6.49 \times 10^{-4}$	$7.50 \times 10^{-4}$	$8.30 \times 10^{-4}$
$I\gamma_{Se}$	$3.54 \times 10^{-6}$	$1.90 \times 10^{-4}$	$2.20 \times 10^{-4}$	$2.43 \times 10^{-4}$
$\varepsilon_{Se}$	$6.09 \times 10^{-5}$	$3.27 \times 10^{-4}$	$3.78 \times 10^{-4}$	$4.18 \times 10^{-4}$
$C_{attn(Al)}$	$1.10 \times 10^{-5}$	$5.89 \times 10^{-5}$	$6.81 \times 10^{-5}$	$7.54 \times 10^{-5}$
$C_{attn(Se)}$	$9.91 \times 10^{-6}$	$5.32 \times 10^{-5}$	$6.15 \times 10^{-5}$	$6.80 \times 10^{-5}$
$^{80}\text{Se}(n, p)^{80}\text{As}$				
Parameters	13.52 MeV	16.86 MeV	19.81 MeV	
$\sigma_{Al}$	$1.27 \times 10^{-4}$	$2.41 \times 10^{-4}$	$2.20 \times 10^{-4}$	
$C_{Se}$	$2.04 \times 10^{-3}$	$2.21 \times 10^{-3}$	$9.94 \times 10^{-4}$	
$AM_{Se}$	$1.59 \times 10^{-9}$	$2.74 \times 10^{-9}$	$2.76 \times 10^{-9}$	
$\lambda_{Se}$	$8.26 \times 10^{-4}$	$1.46 \times 10^{-3}$	$5.26 \times 10^{-4}$	
$W_{Al}$	$1.32 \times 10^{-5}$	$2.04 \times 10^{-5}$	$2.03 \times 10^{-5}$	
$I\gamma_{Al}$	$1.91 \times 10^{-5}$	$3.28 \times 10^{-5}$	$3.31 \times 10^{-5}$	
$\varepsilon_{Al}$	$2.42 \times 10^{-4}$	$4.16 \times 10^{-4}$	$4.19 \times 10^{-4}$	

$C_{Al}$	$3.97 \times 10^{-4}$	$6.96 \times 10^{-4}$	$5.36 \times 10^{-4}$
$AM_{Al}$	$2.36 \times 10^{-9}$	$4.05 \times 10^{-9}$	$4.09 \times 10^{-9}$
$\lambda_{Al}$	$4.49 \times 10^{-7}$	$1.34 \times 10^{-5}$	$7.43 \times 10^{-6}$
$W_{Se}$	$8.14 \times 10^{-7}$	$1.46 \times 10^{-6}$	$1.34 \times 10^{-6}$
$Abun_{Se}$	$2.57 \times 10^{-6}$	$4.41 \times 10^{-6}$	$4.44 \times 10^{-6}$
$I\gamma_{Se}$	$1.52 \times 10^{-5}$	$2.60 \times 10^{-5}$	$2.62 \times 10^{-5}$
$\epsilon_{Se}$	$1.78 \times 10^{-4}$	$3.06 \times 10^{-4}$	$3.08 \times 10^{-4}$
$C_{attn(Al)}$	$4.38 \times 10^{-5}$	$7.52 \times 10^{-5}$	$7.58 \times 10^{-5}$
$C_{attn(Se)}$	$3.96 \times 10^{-5}$	$6.79 \times 10^{-5}$	$6.85 \times 10^{-5}$

**Table 3.24** The calculated covariance and correlation matrix at 10.5, 13.52, 16.86 and 19.81 MeV neutron energies for the  $^{76}\text{Se}(n,p)^{76}\text{As}$ ,  $^{77}\text{Se}(n,p)^{77}\text{As}$ ,  $^{78}\text{Se}(n,p)^{78}\text{As}$  and  $^{80}\text{Se}(n,p)^{80}\text{As}$  reactions cross sections.

Covariance matrix													
3.30													
1.35	1.36												
1.07	2.14	8.55											
9.48	1.89	1.51	4.19										
1.76	1.06	8.45	7.47	2.61									
4.67	3.59	7.41	6.54	2.11	1.86								
4.42	8.81	2.31	6.19	1.99	1.74	8.89							
3.35	6.67	5.31	1.34	1.19	1.05	9.92	1.14						
1.81	1.36	2.85	2.52	3.35	1.13	2.77	2.11	1.65					
2.08	4.15	1.31	2.92	3.87	3.39	1.06	2.43	7.83	1.89				
2.31	4.58	3.65	9.02	4.28	3.75	3.55	7.66	8.66	1.01	2.38			
1.34	1.01	2.12	1.87	2.49	8.42	2.06	1.56	3.18	9.71	1.07	5.11		
2.29	4.58	1.44	3.22	4.27	3.74	1.17	2.69	1.44	6.59	1.85	1.37	7.83	
2.32	4.61	3.67	9.08	4.31	3.77	3.57	7.71	1.45	1.68	5.19	5.98	1.05	1.88
Correlation matrix													

1.0													
0.201	1.0												
0.202	0.198	1.0											
0.255	0.251	0.251	1.0										
0.189	0.056	0.057	0.071	1.0									
0.059	0.226	0.059	0.074	0.095	1.0								
0.082	0.081	0.265	0.102	0.131	0.136	1.0							
0.055	0.054	0.054	0.194	0.069	0.072	0.099	1.0						
0.077	0.287	0.076	0.096	0.051	0.205	0.073	0.049	1.0					
0.083	0.082	0.324	0.104	0.055	0.057	0.258	0.052	0.444	1.0				
0.082	0.081	0.081	0.286	0.054	0.056	0.077	0.147	0.438	0.472	1.0			
0.033	0.121	0.032	0.041	0.022	0.086	0.031	0.021	0.109	0.031	0.031	1.0		
0.045	0.044	0.176	0.056	0.029	0.031	0.139	0.028	0.041	0.171	0.043	0.216	1.0	
0.093	0.091	0.091	0.323	0.061	0.064	0.087	0.166	0.083	0.089	0.246	0.193	0.273	1.0

The uncertainties analysis for the  $^{51}\text{V}(n,p)^{51}\text{Ti}$  reaction were carried out using the covariance method. To avoid neutron flux measurements, a ratio method was used for the cross section calculations. The half-life, isotopic abundance,  $\gamma$ -ray abundance for sample and monitor reaction products with uncertainties are taken from the NNDC nuclear database. The equation (18) was used to calculate the covariance matrix of the  $^{51}\text{V}(n,p)^{51}\text{Ti}$  reaction cross section. The uncertainties of different parameters contribute to the total uncertainty of the measured cross section. The partial uncertainties due to various parameters to obtain cross section are given in Table 3.25 along with their correlations among the three neutron energies. The uncertainties in the measured cross section at different neutron energies were calculated by taking the square root of the respective diagonal element of the covariance matrix. The covariance and correlation matrix of the  $^{51}\text{V}(n,p)^{51}\text{Ti}$  reaction at different energies are presented in Table 3.26.

**Table 3.25** The partial uncertainties and correlations coefficient of various parameters used to obtain the  $^{51}\text{V}(n,p)^{51}\text{Ti}$  reaction cross section.

Parameters	$\langle E_n \rangle = 7.87$ MeV	$\langle E_n \rangle = 13.05$ MeV	$\langle E_n \rangle = 16.98$ MeV	Correlations*
$\sigma_{Al}$	0.2601	0.0624	0.2728	Partially correlated
$C_V$	2.2956	2.9519	3.3589	Uncorrelated
$AM_V$	0.0023	0.0058	0.0052	Fully correlated
$\lambda_V$	0.0415	0.1069	0.0981	Fully correlated
$W_{Al}$	0.0596	0.1913	0.0342	Uncorrelated
$I\gamma_{Al}$	0.0172	0.0445	0.0400	Fully correlated
$\varepsilon_{Al}$	0.4702	1.2152	1.0921	Fully correlated
$f_m$	0.0728	0.1745	0.1868	Uncorrelated
$C_{Al}$	1.1654	1.1229	1.5683	Uncorrelated
$AM_{Al}$	0.0128	0.0330	0.0296	Fully correlated

$\lambda_{Al}$	0.0727	0.1743	0.1866	Fully correlated
$W_V$	0.0084	0.0040	0.0231	Uncorrelated
$Abun_V$	0.0575	0.1487	0.1336	Fully correlated
$I\gamma_V$	0.0493	0.1275	0.1145	Fully correlated
$\varepsilon_V$	0.2656	0.6864	0.6168	fully correlated
$f_u$	0.0779	0.1888	0.1970	Uncorrelated

\*Uncorrelated, fully correlated, and partially correlated mean the correlation coefficient is 0, 1, or between them, respectively. The correlation coefficient for partially correlated are 0.106, 0.036 and 0.202.

**Table 3.26** The calculated covariance and correlation matrix at 7.87, 13.05 and 16.98 MeV neutron energies for the  $^{51}\text{V}(n,p)^{51}\text{Ti}$  reaction cross section.

$\langle E_n \rangle$ (MeV)	Covariance matrix			Correlation matrix		
7.87 (58)	7.012			1.0		
13.05 (68)	0.787	12.105		0.085	1.0	
16.98 (53)	0.709	1.837	15.536	0.068	0.134	1.0

### 3.6 Neutron induced $(n, 2n)$ , $(n, \alpha)$ and $(n, p)$ reactions cross section using the systematic formulae

In a fusion reactor, the hydrogen and helium gases formed due to charged particles reactions  $(n, p)$  and  $(n, \alpha)$  at the fusion reactor wall and affect the reactor structural properties. Similarly, the other reaction leads to atomic displacements and nuclear transmutation, which produces the microstructural effect in the reactor materials. The accurate cross sections around 14-15 MeV energies are needed for structural materials of the fusion reactor, neutron Dosimetry, advance reactor design and shielding for particle accelerators *etc.* These cross sections are also essential for evaluating the nuclear heating rate, primary knock-on atom (PKA) and displacement per atom (DPA) for radiation damage studies. Several empirical formulae exist to predict  $(n, p)$ ,  $(n, 2n)$  and  $(n, \alpha)$  reactions cross sections within 14–15 MeV energies.

It is observed that for many nuclei, a systematic experimental study of 14 MeV neutron induced charged particle reaction cross sections such as  $(n, p)$  and  $(n, \alpha)$  were performed over the years. For many uses, such as studying structural materials of fusion reactors and neutron dosimetry, precise cross sections around 14-15 MeV neutrons are essential for refining nuclear theory. In several areas, the need for fast neutron induced reaction cross

sections data has increased; for example, in biomedical applications such as radioisotopes manufacturing and cancer treatment, accelerator-driven incineration/transmutation of long-lived radioactive nuclear waste (in specific transuranium nuclides) into short-lived or stable isotopes secondary spallation neutron produced by high-intensity, intermediate-energy, charged-particle beams, prolonged planetary space missions, shielding for particle accelerators, material irradiation experiments concerning research and development for fusion reactor technology [16]. Several authors have also suggested several empirical and semi-empirical formulae with various parameters for measurements of  $(n, p)$ ,  $(n, \alpha)$  and  $(n, 2n)$  reactions cross section. These calculated cross sections were discussed and compared with the experimental data near 14.5 MeV neutron energies. The various systematic formulae for  $(n, p)$ ,  $(n, \alpha)$  and  $(n, 2n)$  reactions are given in Tables 3.27, 3.28 and 3.29 respectively [17-34].

**Table 3.27** The systematic formulae for  $(n, p)$  reaction given by the different authors.

Author	Formulae for $(n, p)$ cross section	Mass Region
Levkovski	$\sigma_{n,p} = 50.21 \left( A^{1/3} + 1 \right)^2 \exp \left( - \frac{33.8(N-Z)}{A} \right)$	$40 \leq A \leq 209$
Ait-Tahar	$\sigma_{n,p} = 90.68 \left( A^{1/3} + 1 \right)^2 \exp \left( - \frac{34.48(N-Z+1)}{A} \right)$	$40 \leq A \leq 187$
Doczi	$\sigma_{n,p} = 18.12 \left( A^{1/3} + 1 \right)^2 \exp \left( -19.61 \frac{(N-Z)}{A} + \frac{(N-Z)^2}{A^2} \right)$	$28 \leq A \leq 209$
Kasugai	$\sigma_{n,p} = 1264(N-Z+1) \exp \left( - \frac{46.63(N-Z+1)}{A} \right)$	$28 \leq A \leq 187$
Luo	$\sigma_{n,p} = 62.98 \left( A^{1/3} + 1 \right)^2 \exp \left( -34.45 \frac{(N-Z)}{A} \right)$	$46 \leq A \leq 196$
Forrest	$\sigma_{n,p} = 900 \left( A^{1/3} + 1 \right)^2 \exp \left( -49.27 \frac{(N-Z)}{A} + 197.1 \frac{(N-Z)^2}{A^2} - 0.45A^{1/2} \right)$	$40 \leq A \leq 187$
Bychkov	$\sigma_{n,p} = 7.06\pi r_0^2 \left( A^{1/3} + 1 \right)^2 \exp \left[ \sqrt{\frac{a}{E_n}} \left( \frac{0.58(Z-1)}{A} - \frac{50(N-Z+1)}{A} - 3.26 \right) \right]$	$28 \leq A \leq 209$
Habbani	$\sigma_{n,p} = 20.91 \left( A^{1/3} + 1 \right)^2 \exp \left( -29.53 \frac{(N-Z)}{A} \right)$ $\sigma_{n,p} = 60.34 \left( A^{1/3} + 1 \right)^2 \exp \left( -34.44 \frac{(N-Z+1)}{A} \right)$	$29 \leq A \leq 209$ Odd A $28 \leq A \leq 208$ Even A

C. Konno	$\sigma_{n,p} = 31.42 \left(A^{1/3} + 1\right)^2 \exp\left(-\frac{29.07(N-Z)}{A}\right)$	$40 \leq A \leq 209$
E. Tel	$\sigma_{n,p} = 7.31 \left(A^{1/3} + 1\right)^2 \exp\left(-\frac{20.21(N-Z)}{A}\right)$	$17 \leq A \leq 239$ odd-Z, even-N
Kumabe	$\sigma_{n,p} = 21.8 A \exp\left(-\frac{34(N-Z)}{A}\right)$	$40 \leq A \leq 62$

**Table 3.28** The systematic formulae for  $(n, 2n)$  reaction given by the different authors.

Author	Formulae for $(n, 2n)$ cross section	Mass Region
Chatterjee	$\sigma_{n,2n} = 31.39 \left(A^{1/3} + 1\right)^2 \exp\left(\frac{1.706(N-Z)}{A}\right)$	$45 \leq A \leq 238$
Lu and Fink	$\sigma_{n,2n} = 45.76 \left(A^{1/3} + 1\right)^2 \left[1 - 7.372 \exp\left(-\frac{32.21(N-Z+1)}{A}\right)\right]$	$28 \leq Z \leq 82$
Luo	$\sigma_{n,2n} = 0.0226 \left(A^{1/3} + 1\right)^2 \exp\left(\frac{133.86(N-Z)}{A} - \frac{779.47(N-Z)^2}{A^2} + \frac{1500.51(N-Z)^3}{A^3}\right)$	$23 \leq A \leq 209$
Bychkov	$\sigma_{n,2n} = 8.7(A + 100) \left[1 - 0.88 \exp\left(-\frac{7.95(N-Z)}{A}\right)\right]$	$45 \leq A \leq 238$
Habbani	$\sigma_{n,2n} = 23.53 \left(A^{1/3} + 1\right)^2 \exp\left(3.5 \frac{(N-Z)}{A}\right)$	$45 \leq A \leq 209$ Odd A
	$\sigma_{n,2n} = 20.82 \left(A^{1/3} + 1\right)^2 \exp\left(3.76 \frac{(N-Z+1)}{A}\right)$	$48 \leq A \leq 238$ Even A

**Table 3.29** The systematic formulae for  $(n, \alpha)$  reaction given by the different authors.

Author	Formulae for $(n, \alpha)$ cross section	Mass Region
Levkovski	$\sigma_{n,\alpha} = 16.55 \left(A^{1/3} + 1\right)^2 \exp\left(-\frac{31.26(N-Z)}{A}\right)$	$31 \leq A \leq 202$
Ait-Tahar	$\sigma_{n,\alpha} = 31.66 \left(A^{1/3} + 1\right)^2 \exp\left(-\frac{32.75(N-Z+1)}{A}\right)$	$40 \leq A \leq 188$
Kasugai	$\sigma_{n,\alpha} = 277.86 \exp\left(-\frac{24.66(N-Z)}{A}\right)$	$19 \leq A \leq 187$
Luo	$\sigma_{n,\alpha} = 20.91 \left(A^{1/3} + 1\right)^2 \exp\left(-34.69 \frac{(N-Z)}{A}\right)$	$50 \leq A \leq 206$
Forrest	$\sigma_{n,\alpha} = 24.71 \left(A^{1/3} + 1\right)^2 \exp\left(-19.77 \frac{(N-Z)}{A} + 13.82 \frac{(N-Z)^2}{A^2} - 0.0248A\right)$	$20 \leq Z \leq 50$

Habbani	$\sigma_{n,a} = 3.6 \left( A^{1/3} + 1 \right)^2 \exp \left( -25 \frac{(N-Z-3)}{A} \right)$	286 ≤ A ≤ 238 Even A
Konobeyev	$\sigma_{n,a} = 53.066 \left( A^{1/3} + 1 \right)^2 \exp \left( -209.11S^2 + 8.4723P - \frac{0.19253Z}{A^{1/3}} - 0.96249 \right) \quad Z \leq 50$ $\sigma_{n,a} = 53.066 \left( A^{1/3} + 1 \right)^2 (-1.6462P - 0.39951)^3 \quad Z > 50$ $S = (N - Z + 1)/A, P = (N - Z + 0.95)/A$	40 ≤ A ≤ 209

## Bibliography

- [1] F. P. Brady and J. L. Romero, Nucl. Sci. and Eng. 106, 318-331 (1990).
- [2] C. V. Midhun, M. M. Musthafa, *et al.*, Physical Review C 104, 054606 (2021).
- [3] C. H. Poppe *et al.*, Physical Review C, Vol. 14, Number 2 (1976).
- [4] M. W. McNaughton, N. S. P. King, *et al.*, Nucl. Instr. and Meth. 130, 555-557 (1975).
- [5] D. L. Smith *et al.*, Corrections for Low Energy Neutrons by Spectral Indexing, retrieved from <https://www.oecdnea.org/science/docs/2005/nsc-wpec-doc2005-357.pdf>
- [6] A. Pcelincev, A. Loupilov, *et al.*, Journal of Instrumentation (JINST). Vol.12, May (2017).
- [7] I. Pylypchynets, A. Lengyel *et al.*, Journal of Radioanalytical and Nuclear Chemistry, 319:1315–1319 (2019).
- [8] National Nuclear Data Center (NNDC), NuDat 3.0, <https://www.nndc.bnl.gov/nudat3/>
- [9] R. Capote, K. I. Zolotarev, *et al.*, International Reactor Dosimetry and Fusion File IRDFF v.1.05, IAEA Technical Report No. INDC (NDS)-0616, 9 Oct. (2014).
- [10] Nowotny R., XMuDat: photon attenuation data on PC. IAEA Report IAEA-NDS 195 (1998)
- [11] D. A. Brown, *et al.*, “EDNF/B-VIII.0” Nuclear Data Sheets, 148, 1-142 (2018).
- [12] N. Otuka, B. Lalremruata *et al.*, Radiation Physics and Chemistry Vol. 140, November 2017, Pages 502-510.
- [13] T. Vidmar, EFFTRAN-A Monte Carlo efficiency transfer code for  $\gamma$ -ray spectrometry, Nucl. Instrum. Methods Phys. Res. A 550, 603-608 (2005).
- [14] N. Otuka, R. Capote, *et al.*, EPJ Web of Conferences, 27 00007 (2012).

- [15] L. P. Geraldo and D. L. Smith, Nucl. Instrum. and Methods in Phys. Res. A 290:499–508 (1990).
- [16] Karolina Kolos, Vladimir Sobes *et al.*, Physical Review Research 4, 021001 (2022).
- [17] V.N. Levkovski, Zh. Eksp, Teor. Fiz. 45, 305 (1963).
- [18] S. Ait-Tahar, J. Phys. G: Nucl. Phys. 13, L121 (1987).
- [19] Y. Kasugai, Y. Ikeda, H. Yamamoto, *et al.*, In Proceedings of the 1994 Symposium on Nuclear Data, November 1994, Tokai, Japan.
- [20] R. Doczi, V. Semkova, *et al.*, IAEA-NDS Report No. Indc. (HUN)-032, (1997).
- [21] R. A. Forrest, Report AERE-R-12149. Atomic Energy Research Establishment, Harwell.
- [22] V. M. Bychkov, V. N. Manokhin, *et al.*, IAEA-NDS Report No. Indc. (CCP) 146, (1980).
- [23] J. Luo *et al.*, Nucl. Instrum. Method Phys. Res. B 266, 4862 (2008).
- [24] F. I. Habbani and Khalda T. Osman, Appl. Radiat. Isot. 54, 283 (2001).
- [25] Y. Kasugai, Y. Ikeda, H. Yamamoto, and K. Kawade, in Proceedings of the 1994 Symposium on Nuclear Data, November 1994, Tokai, Japan (JAERI, Ibaraki, 1995).
- [26] J. Luo *et al.*, Nucl. Instrum. Method Phys. Res. B 266, 4862 (2008).
- [27] V. M. Bychkov, V. N. Manokhin, *et al.*, IAEA NDS Report No. Indc. (CCP) 146, (1980).
- [28] F. I. Habbani and Khalda T. Osman, Appl. Radiat. Isot. 54, 283 (2001).
- [29] C. Konno, Y. Ikeda, *et al.*, JAERI Rep. No. 1329, Japan Atomic Energy Research Institute, Tokyo, Japan, (1993).
- [30] E. Tel, B. Sarer, S. Okuducu, *et al.*, J. Phys. G: Nucl. Part. Phys. 29, 2169–2177 (2003).
- [31] I. Kumabe, K. J. Fukuda, Nucl. Sci. Tech. 24, 83 (1987).
- [32] S. Chatterjee, A. Chatterjee, Nucl. Phys. A 125, 593 (1969).
- [33] Wen-deh Lu and R. W. Fink, Phys. Rev. C 4, 1173 (1971).
- [34] A. Yu. Konobeyev, V.P. Lunev, *et al.*, Nucl. Instrum. Methods B 108, 233 (1996).